Spin relaxation in $Cs_2CuCl_{4-x}Br_x$

R. HassanAbadi,[1] R. M. Eremina,[2,3] M. Hemmida,[1] A. Dittl,[1] M. V. Eremin,[3] B. Wolf,[4] W. Assmus,[4]
A. Loidl,[1] and H.-A. Krug von Nidda[1,*]

[1]*Experimentalphysik V, Center for Electronic Correlations and Magnetism, Institute of Physics, Augsburg University,
D-86135 Augsburg, Germany*
[2]*Zavoisky Physical-Technical Institute, Federal Research Center "Kazan Scientific Center of RAS," 420029 Kazan, Russia*
[3]*Institute for Physics, Kazan (Volga region) Federal University, 420008 Kazan, Russia*
[4]*Physikalisches Institut, Goethe-Universität Frankfurt, Max-von-Laue-Strasse 1, 60438 Frankfurt am Main, Germany*

The quantum-spin $S = 1/2$ chain system Cs_2CuCl_4 is of high interest due to competing antiferromagnetic intrachain J and interchain exchange J' interactions and represents a paramount example for Bose-Einstein condensation of magnons [R. Coldea *et al.*, Phys. Rev. Lett. **88**, 137203 (2002)]. Substitution of chlorine by bromine allows tuning the competing exchange interactions and corresponding magnetic frustration. Thereby, anisotropic exchange contributions may be decisive for the resulting ground state. Here we report on electron spin resonance (ESR) in single crystals of $Cs_2CuCl_{4-x}Br_x$ with the aim to analyze the evolution of these anisotropic exchange contributions. The main source of the ESR linewidth is attributed to the uniform Dzyaloshinskii-Moriya interaction. The vector components of the Dzyaloshinskii-Moriya interaction are determined from the angular dependence of the ESR spectra using a high-temperature approximation. The obtained results support the site selectivity of the Br substitution suggested from the evolution of lattice parameters and magnetic susceptibility dependent on the Br concentration.

I. INTRODUCTION

Low-dimensional magnets exhibit a large variety of fascinating ground states, especially in case of competing interactions and geometric frustration [1,2]. All these factors are present in the compounds Cs_2CuCl_4 and Cs_2CuBr_4 [3–5], where antiferromagnetic spin $S = 1/2$ chains of Cu^{2+} ions form triangular antiferromagnetic planes with neighboring chains as depicted in Fig. 1. The orthorhombic crystal structure of both systems belongs to the space group *Pnma* with the room-temperature lattice parameters $a = 9.769$ Å, $b = 7.607$ Å, and $c = 12.381$ Å for Cs_2CuCl_4 [6] and $a = 10.195$ Å, $b = 7.965$ Å, and $c = 12.936$ Å for Cs_2CuBr_4 [5]. The exchange interactions in Cs_2CuCl_4 were estimated from the inelastic neutron-scattering experiments: $J/k_B = 4.34(6)$ K and $J'/k_B = 1.48(6)$ K [7]. Note that the interchain interaction J' is of the same order of magnitude but apparently smaller than the intrachain interaction J [8,9]. In Cs_2CuCl_4 the ratio $J'/J \approx 1/3$ results in formation of a spin-liquid state below about 4 K. Finally, weak interlayer couplings give rise to long-range spin-spiral order below the Néel temperature $T_N = 0.62$ K [8]. For Cs_2CuBr_4 one finds $J/k_B = 14.9$ K and the ratio $J'/J \simeq 0.41$ is larger than in the Cl system indicating a stronger frustration: the field dependence of the magnetization reveals two plateaux [10]. The antiferromagnetic ground state below $T_N = 1.4$ K is interpreted in terms of triplet crystallization [11]. Notably, the discovery of

Bose-Einstein condensation of magnons in Cs_2CuCl_4 in magnetic fields above 8 T triggered a permanent interest in these compounds to date [7,12].

Spinon and magnon excitations in Cs_2CuCl_4 have been studied by magnetic resonance techniques [13–15]. Ultrasound experiments concentrate on the spin-liquid phase and quantum critical behavior [16,17]. A change of the magnetic properties has been reported after application and release of hydrostatic pressure [18], indicating a deformation of the local environment of the copper ions. In Cs_2CuBr_4 the magnetic phase diagram of incommensurate and commensurate structures has been investigated experimentally and theoretically [19,20]. Ultrasound experiments up to magnetic fields of 50 T also suggested the existence of a spin-liquid phase [21], which was supported by the finding of a large zero-field gap even above T_N by high-field electron spin resonance [22].

Chemical substitution of chlorine by bromine allows systematically tuning the exchange coupling between the Cu chains and the strength of frustration [23]. Dependent on the growth conditions in aqueous solution, the whole substitutional series $Cs_2CuCl_{4-x}Br_x$ crystallizes within the same orthorhombic space group *Pnma* at a growth temperature of 50°C, but a water-free tetragonal modification (space group $I4/mmm$), which will not be considered in our present work, is obtained in the range $1 < x < 2$ at a lower growth temperature of 24°C [24]. For the orthorhombic structure the lattice parameters a, b, and c increase linearly with the concentration of bromine ions. Crystallographic and magnetic studies of single crystals of the series $Cs_2CuCl_{4-x}Br_x$ with $0 \leqslant x \leqslant 4$ revealed three different regimes dependent on the bromine concentration x due to site-selective substitution, as there
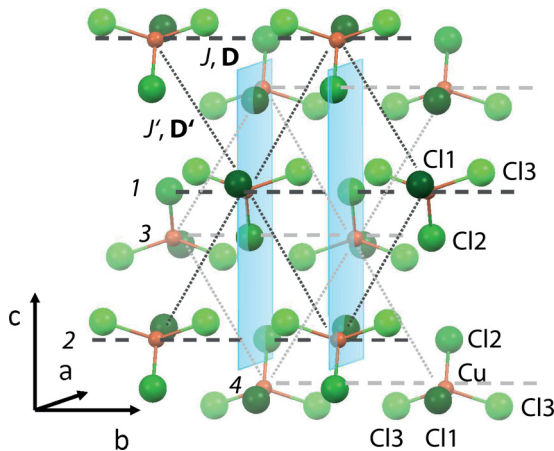
FIG. 1. Crystal structure of $Cs_2CuCl_{4-x}Br_x$ built up from $CuCl_4$ tetrahedra with Cu (small orange spheres), Cl1 (dark green spheres), Cl2 (green spheres), and Cl3 (light green spheres). The Cs ions are omitted for clarity. The relevant intra/interchain exchange (J/J') and DM interactions ($\mathbf{D}/\mathbf{D'}$) are indicated by dashed/dotted lines. The numbers 1–4 mark the four inequivalent chains. The copper $\mathbf{g}$ tensors are equivalent $\mathbf{g}_{\hat{i}}$ on chain 1 and 3, and differ from $\mathbf{g}_{\hat{i}l}$ on chain 2 and 4. The intrachain DM interaction $\mathbf{D}$ attains only 2 nonzero components D_a and D_c within the light blue ac plane, uniform within each chain but alternating with all possible combinations of plus and minus signs between inequivalent chains, while the interchain DM interaction $\mathbf{D'}$ is staggered in all three components.

are three inequivalent Cu–Cl bonds in the distorted $CuCl_4$ tetrahedra. Following the notation of Ref. [23] one finds the longest Cu–Cl1 bond tilted from the a direction, the intermediate Cu–Cl2 bonds tilted from the c direction, and two short Cu–Cl3 bonds involved in the formation of the Cu chains along the b axis. Thus, the larger Br^- anions first substitute the $Cl1^-$ anions with the largest space for $0 \leqslant x \leqslant 1$, then the $Cl2^-$ anions for $1 \leqslant x \leqslant 2$, and finally the $Cl3^-$ anions within the chains for $2 \leqslant x \leqslant 4$. Hence, regarding the x-dependence of the temperature T_{max} of the susceptibility maximum as a measure for the leading exchange J in the spin chains, the following scenario was suggested [23]: for Br substitution on the Cl1 and Cl2 sites, where $T_{max} \approx 3$ K for $x < 2$, the intrachain exchange remains practically unchanged but increases significantly for substitution on the Cl3 sites, where for $x \geqslant 2$ the characteristic temperature increases linearly up to $T_{max} \approx 9$ K at $x = 4$. Recently, the phase diagram has been extended down to lower temperatures by means of neutron scattering experiments [25]. Long-range order was found to be suppressed for the intermediate concentration range $1.5 \leqslant x \leqslant 3.2$. In the same paper, accompanying density functional theory (DFT) calculations suggest a more complex evolution of the exchange integrals J and J' with the bromine content x. Very recent specific heat studies [26] and neutron scattering experiments [27] concentrate on the low-temperature properties in the milli-Kelvin regime with the focus on quantum critical behavior and the crossover of 1D and 2D excitations.

Besides the isotropic exchange interactions, anisotropic exchange contributions like the antisymmetric Dzyaloshinskii-Moriya (DM) interaction play a key role for defining

the ground state of a frustrated magnet. Although these anisotropic interactions are usually at least one or two orders of magnitude weaker than the leading isotropic exchange interactions, they may tip the scales in the subtle balance of competing interactions. Hence, it is very important for the microscopic understanding of the exotic ground states of frustrated magnets to determine the anisotropic exchange components. For this purpose electron spin resonance (ESR) is the method of choice, because the anisotropic interactions drive the spin-spin relaxation and, hence, can be directly derived from the resonance linewidth.

In this report we present an ESR study of the substitutional series $Cs_2CuCl_{4-x}Br_x$. Previously we have shown that in Cs_2CuCl_4 the spin relaxation is governed by the uniform DM interaction within the Cu–Cl chains due to the intrachain Cu–Cl–Cl–Cu bond angle which significantly deviates from $180°$ [28]. From the anisotropy of the resonance linewidth we determined the DM vector in good agreement with antiferromagnetic resonance investigations [29]. Already earlier the DM interaction was found to be essential for the understanding of the excitation spectra not only of Cs_2CuCl_4 but also of Cs_2CuBr_4 [30]. A few years ago, the exchange parameters of both compounds were determined by means of high-field ESR in the ordered phase [31]. Recently, paramagnetic resonance at high frequency in Cs_2CuBr_4 was analyzed [32] to determine the DM interaction following our approach in Cs_2CuCl_4 [32]. Here we perform a comprehensive analysis of the anisotropy of the ESR linewidth in $Cs_2CuCl_{4-x}Br_x$ to determine the evolution of the DM vector dependent on the bromine substitution.

II. EXPERIMENTAL DETAILS

High-quality single crystals of $Cs_2CuCl_{4-x}Br_x$ were grown from aqueous solution by an evaporation technique at a growth temperature of $50°C$ to obtain the proper orthorhombic structure (space group $Pnma$) in the entire concentration range as described in Ref. [24]. All samples were carefully characterized by magnetization and ultrasound measurements [23,33]. ESR measurements were performed in a Bruker ELEXSYS E500 CW-spectrometer at X-band ($\nu \approx 9.36$ GHz) and Q-band frequencies ($\nu \approx 34$ GHz) equipped with continuous He-gas-flow cryostats (Oxford Instruments) covering the temperature range $4.2 \leqslant T \leqslant 300$ K. The single crystals were fixed with well defined orientation in high-purity Suprasil quartz-glass tubes by paraffin and mounted at a computer-controlled goniometer allowing for angular dependent measurements. ESR spectra display the power P absorbed by the sample from the transverse magnetic microwave field as a function of the static magnetic field H. The signal-to-noise ratio of the spectra is improved by recording the derivative dP/dH using lock-in technique with field modulation.

III. RESULTS

In the whole temperature range and for all orientations of the magnetic field H the ESR signal of $Cs_2CuCl_{4-x}Br_x$ consists of a single exchange-narrowed resonance line as exemplarily shown in Fig. 2 for $H \parallel b$. The line is well fitted by
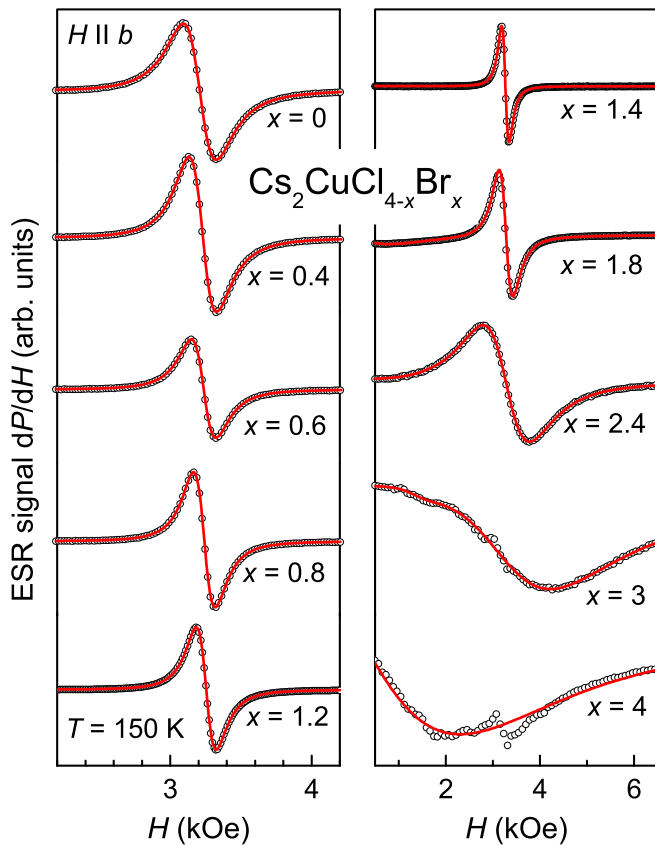
FIG. 2. ESR spectra of Cs$_2$CuCl$_{4-x}$Br$_x$ at selected Br concentrations x for the magnetic field H applied along the crystallographic b axis. The red solid lines indicate the fit by a Lorentzian line shape.

FIG. 3. Temperature dependence of the linewidth ΔH of Cs$_2$CuCl$_{4-x}$Br$_x$ with different Br concentration x for the magnetic field H applied along the crystallographic c axis. The solid lines indicate fits by Eq. (1) containing an Arrhenius law and a critical divergence.

a Lorentz shape at resonance field $H_{\rm res}$ with linewidth HWHM (half width at half maximum) ΔH, indicating that spin-diffusion effects are not relevant in this series of compounds [34,35]. For $x > 1.2$ the linewidth significantly increases with increasing Br concentration, exceeding 2 kOe for $x > 3$. At larger Br concentration the signal becomes too broad to be reasonably evaluated at X-band frequency. This demands high-frequency/high-field ESR investigations as carried out on pure Cs$_2$CuBr$_4$ and reported in Ref. [32]. For spectra, where the linewidth is of the same order of magnitude as the resonance field it was necessary to include the counter resonance at negative resonance field into the fitting to obtain a reasonable description of the resonance signal [36]. The g value is calculated from resonance field and microwave frequency ν via the Larmor condition $h\nu = g\mu_B H_{\rm res}$, where h and μ_B denote Planck constant and Bohr magneton, respectively.

Before discussing the anisotropy of resonance linewidth ΔH and g values in detail, we first focus on the temperature dependence, which is qualitatively similar for all orientations. The evolution of the temperature dependent linewidth and g value with Br concentration x is exemplarily shown in Figs. 3 and 4, respectively, for the magnetic field applied along the crystallographic c axis. As experimental error about $\pm 5\%$ of the absolute value of the linewidth are anticipated both for the linewidth and the resonance-field data. In Fig. 3 for most cases the corresponding error bars would be smaller than the symbol size. For the g values in Fig. 4 the corresponding
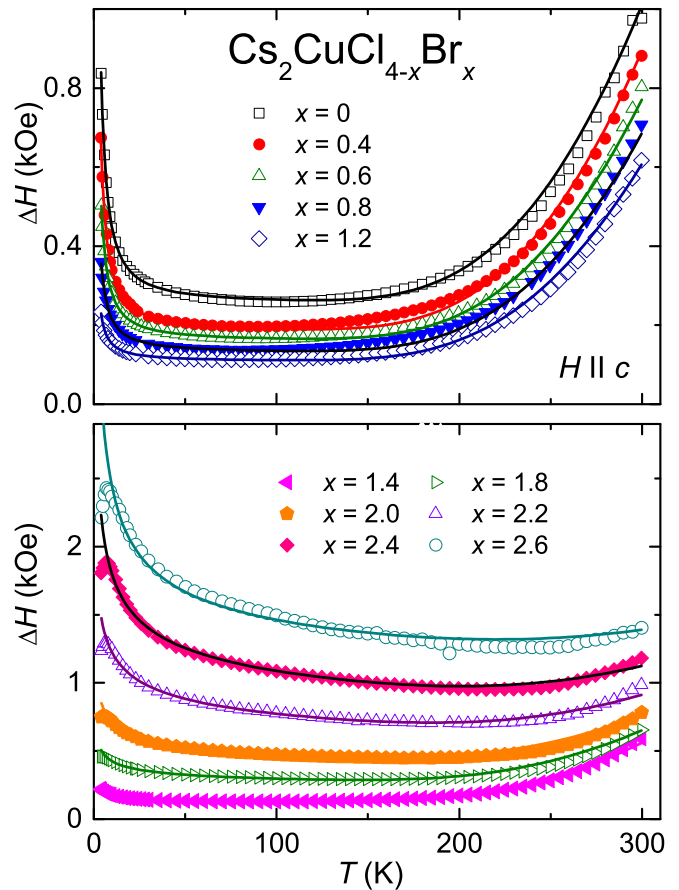
error ranges from $\Delta g \approx 0.003$ in case of $\Delta H = 100$ Oe to $\Delta g \approx 0.06$ for $\Delta H = 2000$ Oe. Error bars have been omitted not to overload the graphs. Like in pure Cs$_2$CuCl$_4$ the linewidth exhibits three temperature regimes with different behavior. For all Br concentrations x the linewidth is only weakly temperature dependent between 50 K and 150 K. It increases following an Arrhenius law $\Delta H \propto \exp(-\Delta/T)$ for high temperatures $T > 150$ K. At low temperatures, for $T < 50$ K the linewidth increases on decreasing temperature approximately by a power law $\Delta H \propto T^{-p}$. For $x \geqslant 2$ a maximum shows up at low temperatures, which limits the description by a power law, and the minimum of the linewidth data shifts to temperatures above 200 K.

The g value is nearly constant and slightly larger than 2 as typical for Cu^{2+} ions in the solid state, where the orbital moment is quenched by the crystal field. Only below 50 K and above 250 K temperature-dependent shifts of several percent occur, which are always negative for high temperatures—here the anisotropy of the **g** tensor diminishes due to thermal excitations—but positive for $x < 0.8$, and again negative for $x > 0.8$ at low temperatures, indicating a change of local field distributions on formation of the ground states for increasing Br concentration.
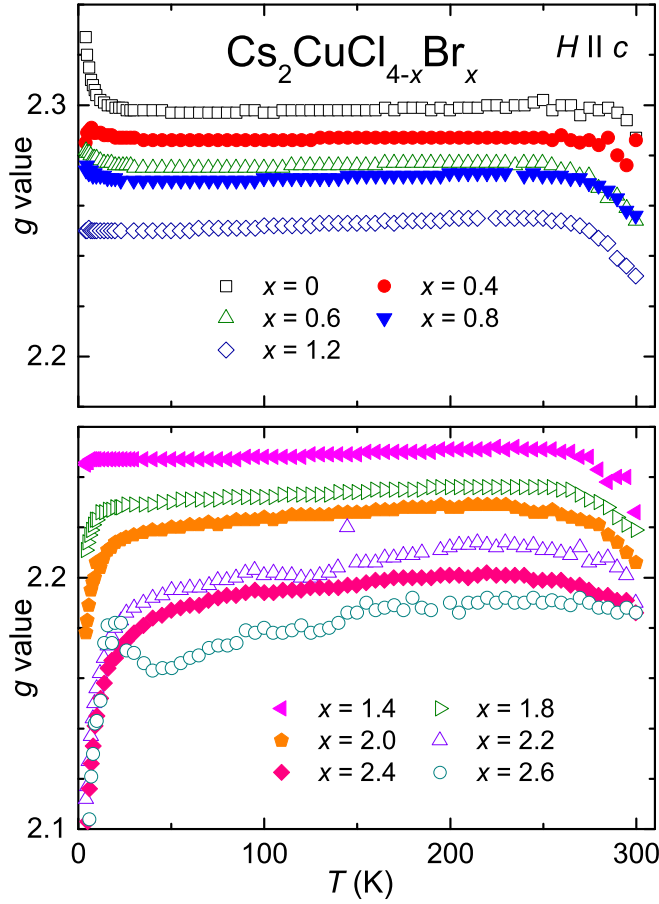
FIG. 4. Temperature dependence of the *g* value of $Cs_2CuCl_{4-x}Br_x$ with different *x* for the magnetic field *H* applied along the crystallographic *c* axis.

For a quantitative evaluation we approximated the temperature dependence of the linewidth data for all three crystallographic axes by the following empirical equation:

$$\Delta H = \Delta H_\infty + \Delta H_{\text{div}} \left(\frac{1\,\text{K}}{T} \right)^p + \Delta H_{\text{act}} \cdot \exp\left(-\Delta/T\right). \quad (1)$$

Here ΔH_∞ denotes the high-temperature asymptotic contribution of pure spin-spin relaxation. The second term accounts for a divergent contribution ΔH_{div} at low temperature with critical exponent *p* normalized to $T = 1$ K, while the last term describes a thermally activated contribution ΔH_{act} characterized by an energy gap Δ. Using both the prefactor ΔH_{act} and the gap value Δ as free parameters turned out to result in strong scattering of both quantities. Hence, we chose a reasonable average value of ΔH_{act} for each orientation as indicated in the caption of Fig. 5, which allowed a simultaneous fit with a single gap value $\Delta(x)$ for each Br-concentration *x*. The corresponding results are shown in Figure 5. While the behavior of ΔH_∞, ΔH_{div} and *p* can be divided into two regimes $x < 1.6$ and $x > 1.6$, the gap value $\Delta(x)$ increases linearly on increasing *x* from 1350 K to approximately 1700 K, as visible in the bottom frame of Fig. 5. This indicates that the activated process is connected to the increase of the average anion mass. In this respect it is important to note that the ESR properties of the crystals start to show irreversible changes on heating
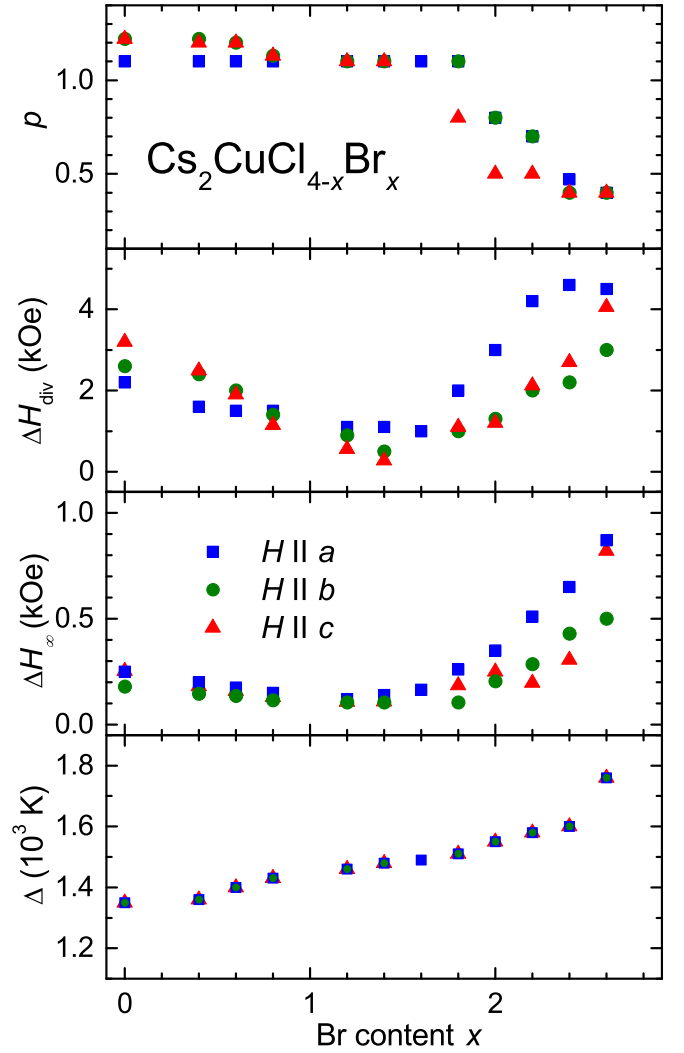

FIG. 5. Concentration dependence of (from top to bottom) low-temperature critical exponent *p* and corresponding divergent linewidth contribution ΔH_{div} as well as constant contribution ΔH_∞ and activation gap Δ with values $\Delta H_{\text{act}}(a) = 67$ kOe, $\Delta H_{\text{act}}(b) = 59$ kOe, $\Delta H_{\text{act}}(c) = 68$ kOe. The parameters are obtained from fitting the linewidth of $Cs_2CuCl_{4-x}Br_x$ by Eq. (1) for the magnetic field *H* applied along the crystallographic *a* (blue squares), *b* (green circles) and *c* axes (red triangles).

above 400 K. Indeed on heating above this temperature, a mass reduction of 0.4% has been reported for Cs_2CuCl_4 which has been ascribed to a partial release of clorine ions from the crystal structure [37]. Thus, the energy gap is probably related to the stability of the compound. Substitution of the chlorine ions by the heavier bromine ions stabilizes the crystal structure, as the release of bromine naturally demands higher energy. The critical exponent *p* remains practically unchanged at $p \approx 1.1$ for $x \leqslant 1.6$, but decreases for $x > 1.6$, where the maximum in the low-temperature linewidth data shows up. The simultaneous change of ΔH_∞ and ΔH_{div} on increasing *x*, i.e., the monotonous decrease for $x \leqslant 1.6$ and the subsequent stronger increase for $x \geqslant 1.6$ indicate that both contributions to the linewidth arise from the Dzyaloshinskii-Moriya interaction for the whole substitutional series, as previously has been
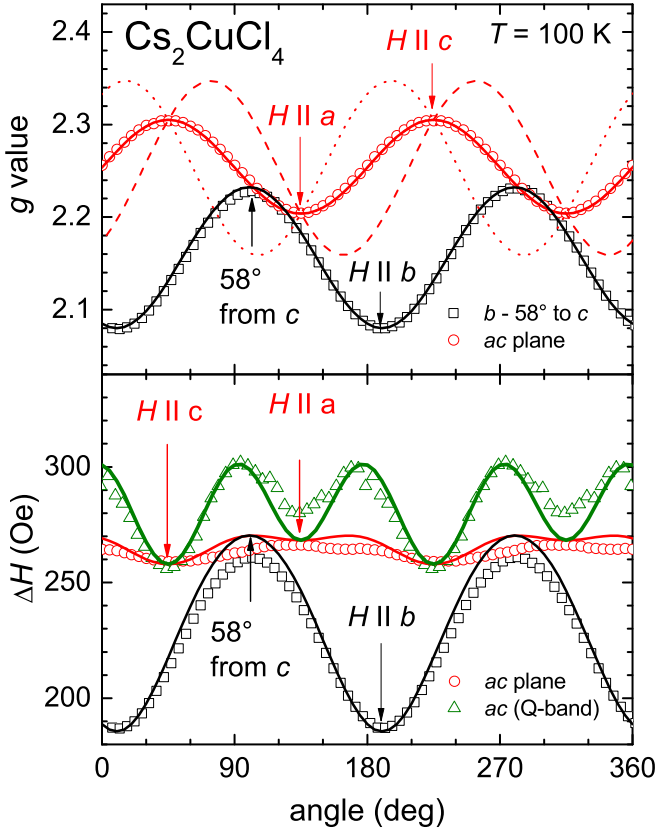
FIG. 6. Angular dependence of g value (upper frame) and linewidth ΔH (lower frame) in Cs$_2$CuCl$_4$ at $T = 100$ K for the magnetic field applied within the ac plane and a perpendicular plane containing the b axis. Black squares and red circles: X-band, green triangles: Q-band. Dashed and dotted lines indicate the two inequivalent **g** tensors, solid lines are fits as described in the text.

FIG. 7. Angular dependence of g value (upper frame) and linewidth ΔH (lower frame) in Cs$_2$CuCl$_{3.6}$Br$_{0.4}$ at $T = 100$ K and X-band frequency for the magnetic field applied within the ac plane and a perpendicular plane containing the b axis. Dashed and dotted lines indicate the two inequivalent **g** tensors, solid lines are fits as described in the text.

derived by detailed temperature dependent calculations for the parent compound Cs$_2$CuCl$_4$ in Ref. [28]. To corroborate this finding, the temperature dependence has been evaluated by the expressions given there in the Appendix.

In the following we will show that the Dzyaloshinskii-Moriya interaction systematically changes with the substitution of Cl by Br, where first the sites outside of the Cu–Cl-Cl–Cu chain are substituted and only for large x the sites within the chain become involved. For this purpose we measured the angular dependence of the g value and linewidth at $T = 100$ K for all Br concentrations under consideration. At this intermediate temperature the line broadening can be treated in high temperature approximation, i.e., $k_B T \gg J$, but the activated process can still be neglected. Figures 6–8 show exemplarily the anisotropies of selected Br concentrations x for the magnetic field applied within the ac plane (red circles) and in a plane containing the b axis (black squares). These geometries have been chosen, because crystals with well defined orientation could be best prepared as platelets cut perpendicular to the chain b axis, or as thin rods grown along the b axis. From the coincidence of both data sets of linewidth and g value one obtains the angle of the rotation plane containing the b axis with respect to the c axis as indicated in Figs. 6–9.
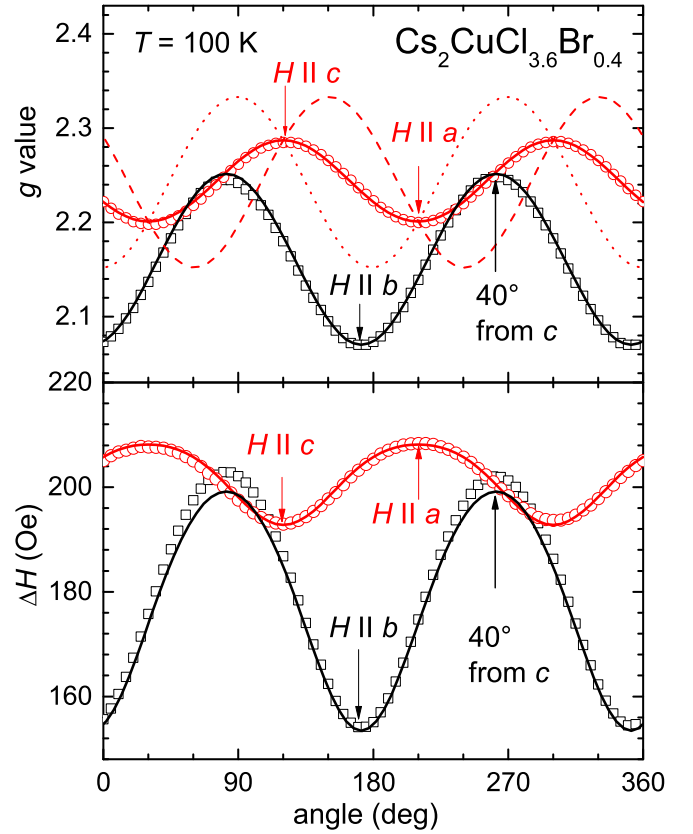
IV. ANALYSIS AND DISCUSSION

To evaluate the anisotropy of the ESR data, the relevant linewidth contributions due to DM interaction and anisotropic Zeeman effect have been derived previously [28] and refined recently [32]. Here we only shortly describe the main steps of the calculation and final expressions.

To derive the contribution of the uniform DM interaction to the linewidth in Cs$_2$CuCl$_{4-x}$Br$_x$, one starts from the one-dimensional Heisenberg Hamiltonian,

$$\mathcal{H} = \sum_i J\mathbf{S}_i \cdot \mathbf{S}_{i+1} + \sum_i \mathbf{D} \cdot [\mathbf{S}_i \times \mathbf{S}_{i+1}] + \mathcal{H}_{\mathrm{inter}}(J', \mathbf{D}'),$$
$$(2)$$

describing the Cu^{2+} spin $S = 1/2$ chains along the crystallographic b axis. Here J is the isotropic antiferromagnetic intrachain superexchange coupling parameter between nearest neighbor spins $\mathbf{S}_i$ and $\mathbf{S}_{i+1}$ within the chains and $\mathbf{D}$ denotes the intrachain DM vector. According to Refs. [38,31], the contribution $\mathcal{H}_{\mathrm{inter}}(J', \mathbf{D}')$ takes the isotropic interchain exchange J' and the interchain DM vector $\mathbf{D}'$ into account, which couple each spin $\mathbf{S}_i$ with two spins on both adjacent chains within the bc plane.

In the crystal structure, there exist four inequivalent chains which differ in the orientation of the corresponding DM
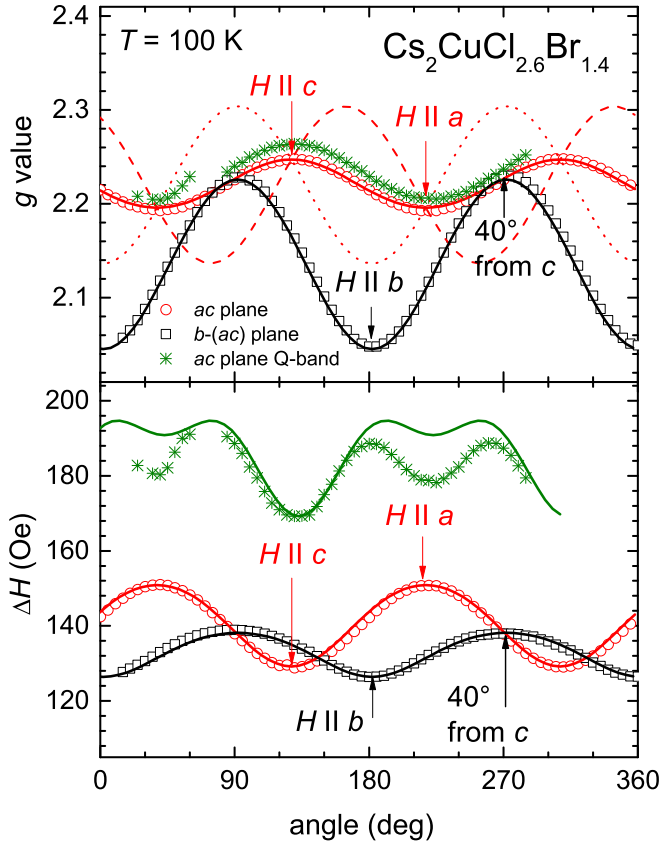
FIG. 8. Angular dependence of g value (upper frame) and linewidth ΔH (lower frame) in $Cs_2CuCl_{2.6}Br_{1.4}$ at $T = 100$ K for the magnetic field applied within the ac plane and a perpendicular plane containing the b axis. Black squares and red circles: X-band, green stars: Q-band. The Q-band data have been measured on a different crystal with slightly larger linewidth. Dashed and dotted lines indicate the two inequivalent **g** tensors, solid lines are fits as described in the text.

FIG. 9. Angular dependence of g value (upper frame) and linewidth ΔH (lower frame) in $Cs_2CuCl_{1.6}Br_{2.4}$ at $T = 100$ K and X-band frequency for the magnetic field applied within the ac plane and a perpendicular plane containing the b axis. Dashed and dotted lines indicate the two inequivalent **g** tensors, solid lines are fits as described in the text.

vector **D** (see Fig. 1). For their description we follow the notations of Starykh *et al.* [38]. The laboratory coordinate system xyz is chosen with the z axis along the externally applied magnetic field. To apply the usual expressions for the transformation of the **D** components between laboratory (xyz) and crystallographic (XYZ) coordinate systems the following notations were used: The Y axis is chosen along the chain (i.e., crystallographic b axis), Z and X axis are parallel to c and a, respectively. Then the components of the DM vector transform following

$$D^x = D^X \cos\beta \cos\alpha + D^Y \cos\beta \sin\alpha - D^Z \sin\beta,$$
$$D^y = D^Y \cos\alpha - D^X \sin\alpha, \qquad (3)$$
$$D^z = D^X \sin\beta \cos\alpha + D^Y \sin\beta \sin\alpha + D^Z \cos\beta,$$

with

$$\cos\alpha = \frac{A}{\sqrt{A^2 + B^2}}, \quad \cos\beta = \frac{C}{\sqrt{A^2 + B^2 + C^2}},$$

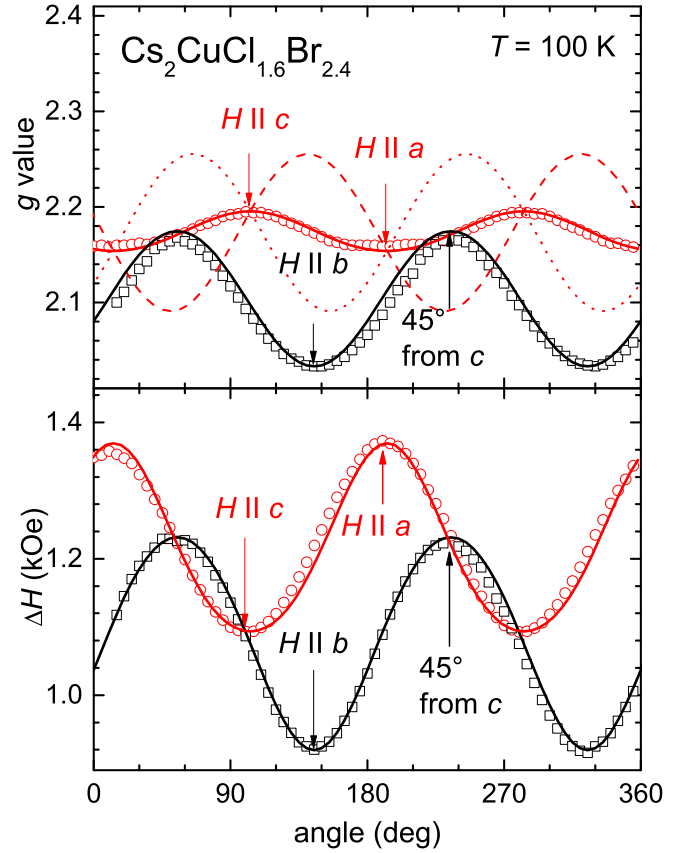and the g value given by

$$g = \sqrt{A^2 + B^2 + C^2},$$

where

$$A = g_{aa} \sin\theta \cos\phi + g_{ab} \sin\theta \sin\phi + g_{ac} \cos\theta,$$
$$B = g_{ba} \sin\theta \cos\phi + g_{bb} \sin\theta \sin\phi + g_{bc} \cos\theta,$$
$$C = g_{ca} \sin\theta \cos\phi + g_{cb} \sin\theta \sin\phi + g_{cc} \cos\theta. \qquad (4)$$

Here, the angles α and β define the orientation of the local coordinate system in which the Hamiltonian of the Zeeman energy $\mathcal{H}_i^{Zee} = \mu_B \mathbf{H} \mathbf{g} \mathbf{S}_i$ takes diagonal form, while θ is the polar angle between external magnetic field and c axis, and ϕ is the azimuthal angle counted from the a direction. $g_{\xi,\eta}$ with $\xi, \eta = a, b, c$ denote the components of the **g** tensor in the crystallographic coordinate system. These transformations are applied for all four chains using the corresponding settings $D_1^X = D_a, D_1^Z = -D_c$ in chain 1, $D_2^X = -D_a, D_2^Z = -D_c$ in chain 2, $D_3^X = -D_a, D_3^Z = D_c$ in chain 3, and $D_4^X = D_a, D_4^Z = D_c$ in chain 4, following the notation of Ref. [38].

Using the theory of exchange narrowing, in the high-temperature limit ($k_B T \gg J$) the angular dependence of the half-width at half maximum ΔH of a single chain is determined by [28,39]

$$\Delta H_{DM} = C \frac{D^2(\theta, \phi) k_B}{\sqrt{\langle J^2 \rangle} g \mu_B} \frac{1}{2\sqrt{2}}. \qquad (5)$$

The parameters D and J are taken in Kelvin, μ_B and k_B denote Bohr magneton and Boltzmann constant, respectively. The prefactor C depends on the cut-off conditions for the spectra and is taken as $C = \pi/\sqrt{2}$ assuming exponential wings. The brackets $\langle J^2 \rangle$ indicate the averaged squared isotropic exchange integral including interchain interactions as described below.

The analogous treatment of the interchain DM vectors $\mathbf{D}'$ and averaging over all four chains results in the same expression like Eq. (5) but with $(\mathbf{D}')^2$ instead of $(\mathbf{D})^2$ in the numerator. Hence, it is not possible to distinguish between intrachain and interchain DM contributions as their squared vector components are just summed up. Therefore, in the following we will omit the prime in the notation of the experimentally determined DM components, however keeping in mind that for symmetry reasons nonzero b-components do not arise from intrachain exchange.

Note that there are two magnetically nonequivalent Cu^{2+} positions with different orientation of the $\mathbf{g}$ tensor within the ac plane, i.e., $\mathbf{g}_I$ and $\mathbf{g}_{II}$, in the unit cell, but within a single chain all $\mathbf{g}$ tensors are equivalent. Details can be found in Ref. [28]. The effective g value for a certain magnetic field direction is given by the arithmetic average $g = (g_I + g_{II})/2$ of the local g values of the two magnetically inequivalent Cu sites in the crystal structure (dashed and dotted lines in the upper frames of Figs. 6–8). Supporting measurements of the linewidth anisotropy in the ac plane have been performed at Q-band frequency for some of the crystals to crosscheck the local $\mathbf{g}$ tensors based on the line broadening due to the anisotropic Zeeman effect, given by

$$\Delta H_{\mathrm{AZ}} = \left(\frac{g_I - g_{II}}{g} \right)^2 \frac{g \mu_B H_{\mathrm{res}}^2}{\sqrt{\langle J^2 \rangle}}, \qquad (6)$$

which results in the 90° modulation (green triangles/stars in the lower frames shown in Figs. 6 and 8). Here $\langle J^2 \rangle = [J^2 + 2(J')^2]/3$ denotes the averaged squared exchange integral consisting of one nearest neighbor contribution J within the chain and two links J' to the neighboring chain due to the triangular structure. The dependence of the local $\mathbf{g}$ tensor on the Br content is depicted in the top frame of Fig. 10. After refined evaluation of the data the absolute values of the local $\mathbf{g}$ tensor components obtained for $x = 0$ have been improved as compared to those values obtained earlier in Ref. [28]. The principal values simultaneously slightly decrease on increasing x, while the sequence $g_1 > g_2 > g_3$ remains conserved.

To describe the experimentally observed angular dependence of the linewidth, we averaged the DM contributions Eq. (5) of all four inequivalent chains plus the anisotropic Zeeman contribution Eq. (6) due to the different orientation of the $\mathbf{g}$ tensors of the two magnetically inequivalent copper sites. For the perpendicular plane the anisotropic Zeeman contribution is of minor importance. From the angular dependence of the linewidth we obtained the components of the DM vector as well as—under simultaneous consideration of the temperature dependence of the linewidth (cf. Appendix)—the effective exchange parameter $J_{\mathrm{eff}} = \sqrt{\langle J^2 \rangle}$, respectively. Note that regarding Eqs. (5) and (6), only the average of the squared exchange parameters accounts for the exchange narrowing of the ESR signal. Therefore, we obtain only absolute values of
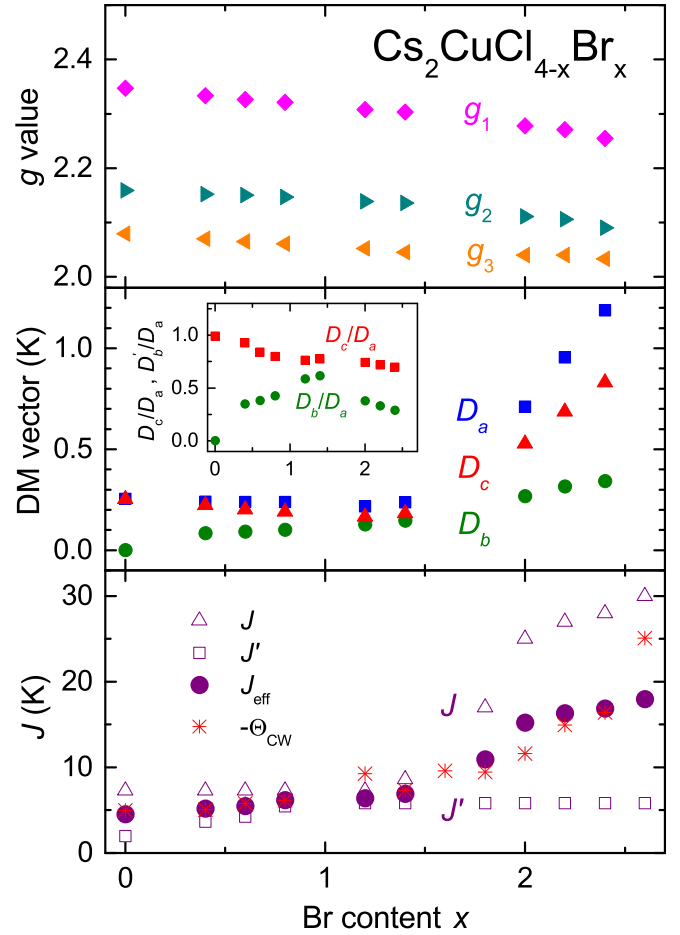

FIG. 10. Top frame: bromine-concentration dependence of the diagonal components of the $\mathbf{g}$ tensor in local coordinates. Middle frame: DM-vector components and ratio of DM components (inset). Bottom frame: Intrachain J, interchain J', and resulting effective exchange parameter $J_{\mathrm{eff}} = \sqrt{\langle J^2 \rangle}$ of Cs$_2$CuCl$_{4-x}$Br$_x$. The Curie-Weiss temperature Θ obtained from the temperature dependence of the spin susceptibility is shown for comparison. The absolute values of the exchange interactions and squared DM vectors may vary within a factor of about 2 dependent on the chosen cutoff condition [40].

the effective exchange parameter. Thus, we are not sensitive to a change of sign, i.e., we cannot distinguish between ferro- and antiferromagnetic exchange. Moreover, without further assumptions it is impossible to distinguish a change in J' from a change in J. Here we use the information obtained from the x dependence of T_{max} in the magnetic susceptibility [23].

The evolution of the DM vector with increasing x is shown in the middle frame of Fig. 10. For $x = 0$, we find $D_a \simeq D_c$ while the component $D_b = 0$ in agreement with the results obtained in Ref. [28]. For $x < 1.6$, both D_a and D_c change only slightly, but D_b becomes nonzero and gradually increases on increasing x. For $x > 1.6$, the DM components D_a and D_c rapidly increase, while D_b continues with the same slope as for $x < 1.6$. The observed changes are in line with the site selective substitution of Cl by Br, D_a and D_c depend on the Cu–Cl–Cl–Cu bond within the chains. Therefore, they remain nearly unchanged at low Br content x when Br substitutes only Cl sites outside the chains, but strongly increase for
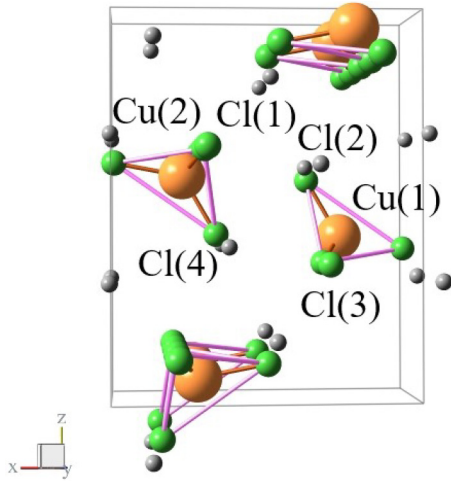
FIG. 11. View of the crystal structure of $Cs_2CuCl_{4-x}Br_x$ along the b direction (Cu large orange, Cl middle green, and Cs small grey spheres) to illustrate possible superexchange paths between copper ions Cu(1) and Cu(2) of neighboring chains of adjacent bc layers. Note that the numbering of the Cl ions just counts the possible exchange bridges independent from the notation of nonequivalent Cl sites used in Fig. 1.

substitution within the chains. Notably the effective exchange J_{eff} increases for $0 \leqslant x \leqslant 1$ from about 4 to 7 K, due to the increase of the interchain coupling J' on substitution of Cl1 sites by Br from $J' = 0.3J$ for $x = 0$ to $J' = 0.8J$ for $x = 1$. Such a change from one-dimensional to two-dimensional character at intermediate Br concentrations x is in fair agreement with recent specific-heat results [26]. In the same range of x the ratio D_c/D_a decreases from 1 down to 0.75. For further increasing x both quantities change only slightly when the Cl2 sites are substituted by Br. For $x > 1.6$ a strong increase of J_{eff} is inferred from the temperature dependence of the linewidth in agreement with the susceptibility, as the Br ions substituted within the chains obviously strongly increase the intrachain exchange. Such an increase of the intrachain exchange is in agreement with the increase of the temperature, where the characteristic maximum of the spin-chain susceptibility is located, from 3 K at $x = 1.6$ up to 9 K for $x = 4$ as documented in Ref. [23]. This is also in accordance with comparative antiferromagnetic resonance experiments [31] on the pure compounds $x = 0$ and $x = 4$ yielding $J(x = 4)/J(x = 0) \approx 3$ and $J'(x = 4)/J'(x = 0) \approx 4$. Regarding the DM interaction, for $x > 2.4$ the ratio D_c/D_a is expected to decrease gradually down to the value $D_c/D_a = 0.3$ reported for the pure Br compound [31,32].

Finally we consider the ratio D_b/D_a, which increases for $x < 1.6$ but decreases for larger x. This indicates that the appearance of sizable contributions D_b indeed is connected to a certain amount of disorder. To understand how disorder can generate DM contributions along the b axis, we consider the exchange bonds of two Cu ions Cu(1) and Cu(2) in adjacent chains of neighboring bc planes as indicated in Fig. 11. The distance between them is 6.793 Å. The superexchange interaction between the copper ions is transferred via intermediate chlorine ions with numbers 1, 2, 3, and 4. According to rules outlined by Keffer [41] and Moskvin [42], the Dzyaloshinskii-

TABLE I. Bond lengths of the interchain superexchange paths in Cs_2CuCl_4.

Bridge j	$R[Cu(1)–Cl(j)]$ (Å)	$R[Cu(2)–Cl(j)]$ (Å)
1	5.7088	2.2130
2	2.1473	5.6649
3	2.2127	5.7096
4	5.6640	2.1478

Moriya vector is defined by the expression

$$\mathbf{D}_{12} = \sum_j \mathbf{D}_{12}^{(j)}[\mathbf{n}_{1j} \times \mathbf{n}_{2j}]$$

$$= \sum_j \left(D_a^{(j)}\mathbf{n}_a^{(j)} + D_b^{(j)}\mathbf{n}_b^{(j)} + D_c^{(j)}\mathbf{n}_c^{(j)} \right), \quad (7)$$

where the index j corresponds to the position of chlorine ions and the unit vectors $\mathbf{n}_{1j}$ and $\mathbf{n}_{2j}$ point from Cl(j) to Cu(1) and Cu(2), respectively. As can be seen from the Fig. 11 between the two copper ions Cu(1) and Cu(2) there are four bridges of superexchange bonds with interion distances given for Cs_2CuCl_4 in Table I. Since the interion distances in the bridges 1 and 3 as well as in 2 and 4 are the same with high accuracy, it is natural to assume that $|D_\alpha^{(1)}| = |D_\alpha^{(3)}|$ and $|D_\alpha^{(2)}| = |D_\alpha^{(4)}|$ for all three components $\alpha = a, b, c$.

In this case, as can be seen from the comparison of the first and third (second and fourth) columns of Table II, the contributions to the DM vector are compensated in pairs. However, in $Cs_2CuCl_{4-x}Br_x$ crystals, the noted compensation is violated. Thus, if for example a Cl(1) ion is replaced with a Br(1) ion, then the channels of exchange coupling through Br(1) and Cl(3) will no longer compensate each other. As a result, all three components of the DM vector will be nonzero. It is also clear that, when all Cl ions are completely replaced by Br ions, as is implemented in Cs_2CuBr_4 crystals, the compensation of DM contributions is restored and the component of the DM vector along the b axis is lost again, as observed in ESR experiments on Cs_2CuBr_4 [32].

Let us note also another variant of the analysis of the peculiarities of the DM interaction between ions Cu(1) and Cu(2). The distance between Cl(1) and Cl(2) ions as well as between Cl(3) and Cl(4) is just 4.105 Å. This approximately corresponds to the sum of the ionic radii (1.81 Å) of chlorine ions. In this connection, pairs of Cl(1) and Cl(2) as well as of Cl(3) and Cl(4) ions can be considered as "molecules" through which the superexchange coupling between the copper ions Cu(1) and Cu(2) is transferred. In this case, instead of four bridges, we have only two, therefore the situation becomes more clear. If these bridges are formed by the same ions, then their contributions to the DM vector compensate each

TABLE II. Calculated values of vector components $\mathbf{n}_{1j} \times \mathbf{n}_{2j}$.

$\mathbf{n}_{1j} \times \mathbf{n}_{2j}$	Cl(1)	Cl(2)	Cl(3)	Cl(4)
$n_a^{(j)}$	0.5548	0.5818	−0.5548	−0.5817
$n_b^{(j)}$	−0.4504	−0.6305	0.4502	0.6303
$n_s^{(j)}$	−0.6094	−0.3356	0.6097	0.3359

other, but under partial replacement of the CI ions by Br the compensation is violated.

V. CONCLUSION

Our comprehensive electron-spin-resonance investigation of the substitutional series Cs$_2$CuCl$_{4-x}$Br$_x$ provides important microscopic information on the evolution of local exchange couplings and relaxation channels in this frustrated quantum-spin $S = 1/2$ chain compound. The simultaneous evaluation of the anisotropy of g value and linewidth taking into account the anisotropic Zeeman effect allows to determine the anisotropic exchange contributions. Starting from $x = 0$ the Dzyaloshinskii-Moriya (DM) interaction provides the dominant relaxation channel with the DM vector oriented within the ac plane with an angle of about 45° with respect to the a axis. On increasing x, the DM vector gradually rotates to approximately 35° within the ac plane for high x. The absolute value of the DM vector changes only slightly for $x < 1.6$ but increases significantly for $x > 1.6$, when Br ions mainly substitute Cl ions within the chains. Contributions of the DM vector along the b direction can be explained in terms of disorder on the anion sites which destroys inversion symmetry

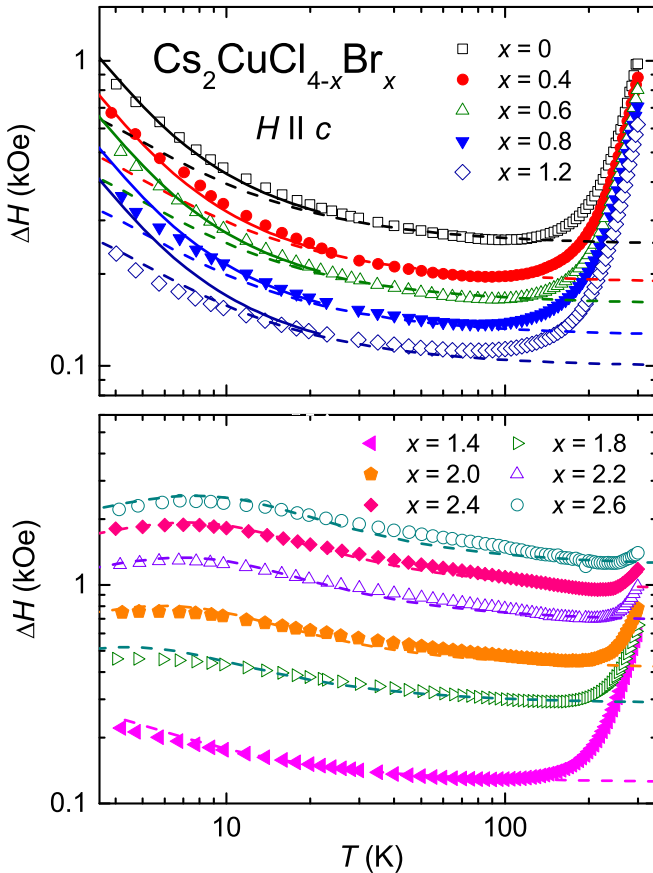of the binding geometry and thus inhibits the compensation of corresponding DM components.

FIG. 12. Temperature dependence of the linewidth ΔH of Cs$_2$CuCl$_{4-x}$Br$_x$ with different Br concentration x for the magnetic field H applied along the crystallographic c axis. Solid and dashed lines indicate fits by the quantum approach and by the classical approximation for the spin relaxation via uniform DM interaction in a spin 1/2 chain, respectively.
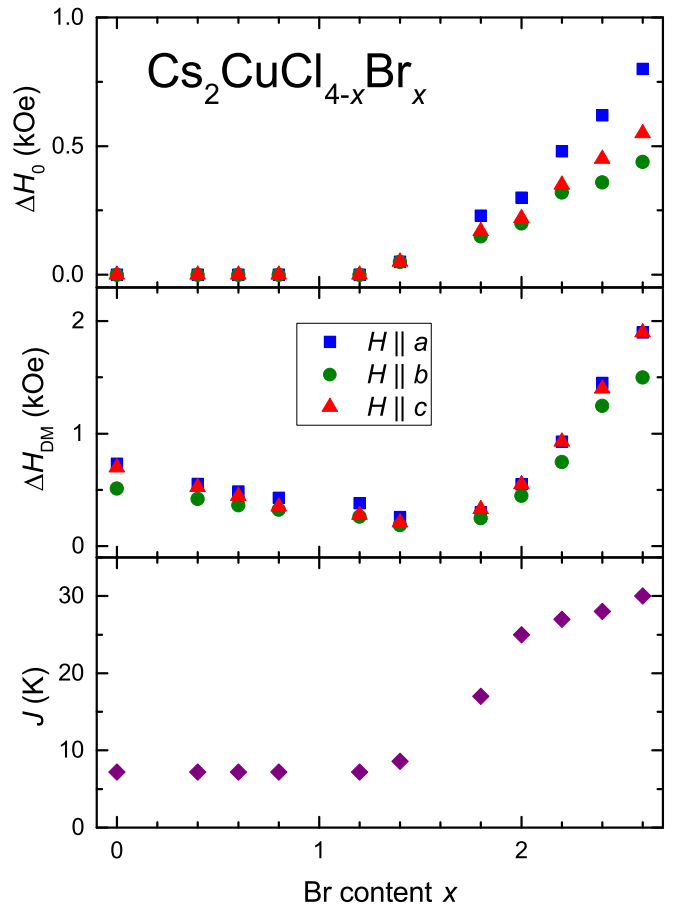

FIG. 13. Concentration dependence of (from top to bottom) residual linewidth ΔH_0, uniform DM linewidth contribution ΔH_{DM}, and intrachain exchange J of Cs$_2$CuCl$_{4-x}$Br$_x$ obtained from the temperature dependence of the ESR linewidth using the approach derived in Ref [28].

APPENDIX: SPIN RELAXATION VIA DM INTERACTION

For a deeper analysis of the temperature dependent linewidth data we use the expressions derived previously [28] for the spin relaxation in pure Cs_2CuCl_4 due to the presence of the uniform DM interaction along the Cu chains. As illustrated in Fig. 12, we compare the applicability of both the quasiclassical (dashed lines) as well as the quantum approach (solid lines). It turns out that the quantum approach works well for bromine concentrations $0 \leqslant x \leqslant 0.6$. For $x = 0.8$ the experimental data are found between quantum and quasiclassical description, but for $x \geqslant 1.2$ the quasiclassical expression turns out to be preferable. For $x \geqslant 1.4$ an additional temperature-independent contribution has to be added to obtain a satisfactory agreement with the data. Note that the maximum, which appears in the temperature dependence for $x \geqslant 1.8$ is directly related to the intrachain exchange J.

The fit results obtained from the temperature dependent linewidth data for the magnetic field applied along all three main axes of the orthorhombic crystal structure are depicted in Fig. 13. The middle frame shows the DM derived linewidth contribution ΔH_{DM}, which decreases approximately linearly on increasing x up to $x = 1.4$, but significantly increases above $x = 1.8$. The intrachain exchange J, which one can see in the bottom frame, is practically unchanged up to $x = 1.2$, but increases by a factor of approximately 3 in the range $1.4 \leqslant$

$x \leqslant 2$, followed by a weaker increase for $x > 2$. Note that the absolute values are somewhat larger than the literature values, which is related to the choice of the cut-off conditions for the correlation function. The temperature-independent residual linewidth contribution ΔH_0, shown in the top frame, is not relevant for $x \leqslant 1.2$, but it was necessary to be added to the expressions given in Ref. [28] to obtain a satisfactory fit of the data at larger x. Obviously this is related to the disorder induced by Br substitution. Although, ΔH_0 reveals a linear increase to higher bromine content, it has to be noted that its relative contribution $\Delta H_0/\Delta H_{DM}$ decreases by a factor of about 3 in the range $1.8 \leqslant x \leqslant 2.6$. Comparison with our empirical fitting by Eq. (1) shows that the x dependence of ΔH_{DM} is in nice agreement with that of ΔH_∞ and corresponding ΔH_{div} corroborating their common origin in the DM interaction. The decrease of the critical exponent p observed for $x > 1.6$ is related to the appearance of the linewidth maximum and the corresponding increase of the intrachain exchange J in the same bromine-concentration range.

In general, the fact that for elevated x the quasiclassical approach is applicable rather than the quantum approach and at the same time the residual linewidth becomes sizable, indicates that disorder and the resulting distribution of exchange bonds within and between the chains plays an important role for the physical properties in this range of Br content.

---

[1] A. Vasiliev, O. Volkova, E. Zvereva, and M. Markina, Quantum Mater. **3**, 18 (2018).

[2] L. Balents, Nature **464**, 199 (2010).

[3] D. P. Mellor, Z. Krist. **101**, 160 (1939).

[4] L. Helmholz and R. F. Kruh, J. Am. Chem. Soc. **74**, 1176 (1952).

[5] B. Morosin and E. C. Lingafelter, Acta Crystallogr. **13**, 807 (1960).

[6] S. Bailleul, D. Svoronos, P. Porchner, and A. Tomas, C. R. Acad. Sci. Ser. II **313**, 1149 (1991).

[7] R. Coldea, D. A. Tennant, K. Habicht, P. Smeibidl, C. Wolters, and Z. Tylczynski, Phys. Rev. Lett. **88**, 137203 (2002).

[8] R. Coldea, D. A. Tennant, A. M. Tsvelik, and Z. Tylczynski, Phys. Rev. Lett. **86**, 1335 (2001).

[9] O. A. Starykh and L. Balents, Phys. Rev. Lett. **98**, 077205 (2007).

[10] T. Ono, H. Tanaka, O. Kolomiyets, H. Mitamura, T. Goto, K. Nakajima, A. Oosawa, Y. Koike, K. Kakurai, J. Klenke, P. Smeibidle, and M. Meißner, J. Phys.: Condens. Matter **16**, S773 (2004).

[11] T. Ono, H. Tanaka, H. Aruga Katori, F. Ishikawa, H. Mitamura, and T. Goto, Phys. Rev. B **67**, 104431 (2003).

[12] T. Radu, H. Wilhelm, V. Yushankhai, D. Kovrizhin, R. Coldea, Z. Tylczynski, T. Luhmann, and F. Steglich, Phys. Rev. Lett. **95**, 127202 (2005).

[13] M.-A. Vachon, G. Koutroulakis, V. F. Mitrovic, O. Ma, J. B. Marston, A. P. Reyes, P. Kuhns, R. Coldea, and Z. Tylczynski, New J. Phys. **13**, 093029 (2011).

[14] A. I. Smirnov, K. Y. Povarov, S. V. Petrov, and A. Y. Shapiro, Phys. Rev. B **85**, 184423 (2012).

[15] A. I. Smirnov, T. A. Soldatov, K. Yu. Povarov, and A. Ya. Shapiro, Phys. Rev. B **91**, 174412 (2015).

[16] S. Streib, P. Kopietz, P. T. Cong, B. Wolf, M. Lang, N. van Well, F. Ritter, and W. Assmus, Phys. Rev B **91**, 041108(R) (2015).

[17] P. T. Cong, L. Postulka, B. Wolf, N. van Well, F. Ritter, W. Assmus, C. Krellner, and M. Lang, J. Appl. Phys. **120**, 142113 (2016).

[18] Hyeong-Jin Kim, C. R. S. Haines, C. Liu, Sae Hwan Chun, Kee Hoon Kim, H. T. Yi, S.-W. Cheong, and S. S. Saxena, Low Temp. Phys. **43**, 901 (2017).

[19] Y. Fujii, H. Hashimoto, Y. Yasuda, H. Kikuchi, M. Chiba, S. Matsubara, and M. Takigawa, J. Phys.: Condens. Matter **19**, 145237 (2007).

[20] J. Alicea, A. V. Chubukov, and O. A. Starykh, Phys. Rev. Lett. **102**, 137201 (2009).

[21] B. Wolf, P. T. Cong, N. Krüger, F. Ritter, W. Assmus, and M. Lang, J. Low Temp. Phys. **170**, 236 (2013).

[22] S. A. Zvyagin, M. Ozerov, D. Kamenskyi, J. Wosnitza, J. Krzystek, D. Yoshizawa, M. Hagiwara, R. Hu, H. Ryu, C. Petrovic, and M. E. Zhitomirsky, New J. Phys. **17**, 113059 (2015).

[23] P. T. Cong, B. Wolf, M. de Souza, N. Krüger, A. A. Haghighirad, S. Gottlieb-Schoenmeyer, F. Ritter, W. Assmus, I. Opahle, K. Foyevtsova, H. O. Jeschke, R. Valenti, L. Wiehl, and M. Lang, Phys. Rev. B **83**, 064425 (2011).

[24] N. Krüger, S. Belz, F. Schossau, A. A. Haghighirad, P. T. Cong, B. Wolf, S. Gottlieb-Schoenmeyer, F. Ritter, and W. Assmus, Cryst. Growth Des. **10**, 4456 (2010).

[25] N. van Well, O. Zaharko, B. Delley, M. Skoulatos, R. Georgii, S. van Smaalen, and Ch. Rüegg, Ann. der Phys. **530**, 1800270 (2018).

[26] U. Tutsch, O. Tsyplyatyev, M. Kuhnt, L. Postulka, B. Wolf, P. T. Cong, F. Ritter, C. Krellner, W. Assmus, B. Schmidt,

P. Thalmeier, P. Kopietz, and M. Lang, Phys. Rev. Lett. **123**, 147202 (2019).

[27] N. van Well, S. Ramakrishnan, K. Beauvois, N. Qureshi, E. Ressouche, M. Skoulatos, R. Georgii, O. Zaharko, and S. van Smaalen, Ann. der Phys. **532**, 2000147 (2020).

[28] M. A. Fayzullin, R. M. Eremina, M. V. Eremin, A. Dittl, N. van Well, F. Ritter, W. Assmus, J. Deisenhofer, H.-A. Krug von Nidda, and A. Loidl, Phys. Rev. B **88**, 174421 (2013).

[29] K. Y. Povarov, A. I. Smirnov, O. A. Starykh, S. V. Petrov, and A. Y. Shapiro, Phys. Rev. Lett. **107**, 037204 (2011).

[30] J. O. Fjaerestad, W. Zheng, R. R. P. Singh, R. H. McKenzie, and R. Coldea, Phys. Rev. B **75**, 174447 (2007).

[31] S. A. Zvyagin, D. Kamenskyi, M. Ozerov, J. Wosnitza, M. Ikeda, T. Fujita, M. Hagiwara, A. I. Smirnov, T. A. Soldatov, A. Ya. Shapiro, J. Krzystek, R. Hu, H. Ryu, C. Petrovic, and M. E. Zhitomirsky, Phys. Rev. Lett. **112**, 077206 (2014).

[32] E. Schulze, A. N. Ponomaryov, J. Wosnitza, H. Tanaka, and S. A. Zvyagin, Low Temp. Phys. **43**, 1311 (2017).

[33] A. Kreisel, P. Kopietz, P. T. Cong, B. Wolf, and M. Lang, Phys. Rev. B **84**, 024414 (2011).

[34] R. E. Dietz, F. R. Merrit, R. Dingle, D. Hone, B. G. Silbernagel, and P. M. Richards, Phys. Rev. Lett. **26**, 1186 (1971).

[35] M. J. Hennessey, C. D. McElwee, and P. M. Richards, Phys. Rev. B **7**, 930 (1973).

[36] J. P. Joshi and S. V. Bhat, J. Magn. Reson. **168**, 284 (2004).

[37] Z. Tylczynski, P. Piskunowicz, A. N. Nasyrov, A. D. Karaev, Kh. T. Shodiev, and G. Gulamov, Phys. Stat. Sol. (a) **133**, 33 (1992).

[38] O. A. Starykh, H. Katsura, and L. Balents, Phys. Rev. B **82**, 014421 (2010).

[39] R. Kubo and K. Tomita, J. Phys. Soc. Jpn. **9**, 888 (1954).

[40] T. G. Castner and M. Seehra, Phys. Rev. B **4**, 38 (1971).

[41] F. Keffer, Phys. Rev. **126**, 896 (1962).

[42] A. S. Moskvin, Condens. Matter **4**, 84 (2019).